Journal of Colloid and Interface Science 607 (2022) 655–661

Contents lists available at ScienceDirect

Journal of Colloid and Interface Science

journal homepage: www.elsevier.com/locate/jcis

CoS_2-TiO_2@C Core-Shell fibers as cathode host material for High-Performance Lithium-Sulfur batteries

Dianming Li [a], Hongtai Li [b], Shumin Zheng [b], Ning Gao [b], Shuai Li [a], Jing Liu [a], Lanlan Hou [a], Jingchong Liu [a], Beibei Miao [c], Jie Bai [c], Zhimin Cui [a], Nü Wang [a,*], Bao Wang [b,*], Yong Zhao [a,*]

[a] Key Laboratory of Bioinspired Smart Interfacial Science and Technology of Ministry of Education, School of Chemistry, Beihang University, Beijing 100191, PR China
[b] State Key Laboratory of Biochemical Engineering, Institute of Process Engineering, Chinese Academy of Sciences, Beijing 100190, PR China
[c] Chemical Engineering College, Inner Mongolia University of Technology, Huhhot 010051, PR China

GRAPHICAL ABSTRACT

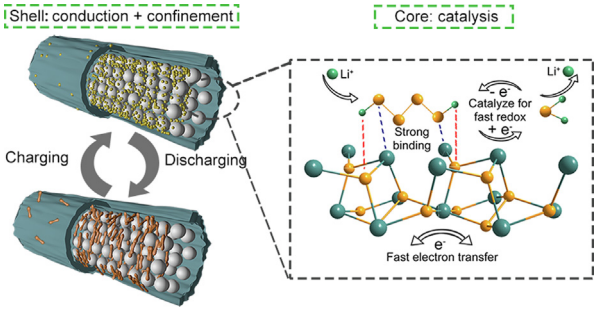

ARTICLE INFO

Article history:
Received 10 June 2021
Revised 24 August 2021
Accepted 25 August 2021
Available online 28 August 2021

Keywords:
Lithium-sulfur batteries
Coaxial electrospinning
Core–shell fibers
Energy

ABSTRACT

Owing to the low cost, high energy density, and high theoretical specific capacity, lithium-sulfur batteries have been deemed as a potential choice for future energy storage devices. However, they also have suffered from several scientific and technical issues including low conductivity, polysulfides migration, and volume changes. In this study, CoS_2-TiO_2@carbon core–shell fibers were fabricated through combination of coaxial electrospinning and selective vulcanization method. The core–shell fibers are able to efficiently host sulfur, confine polysulfides, and accelerate intermediates conversion. This electrode delivers an initial specific capacity of 1181.1 mAh g^{-1} and a high capacity of 736.5 mAh g^{-1} after 300 cycles with high coulombic efficiency over 99.5% (capacity decay of 0.06% per cycle). This strategy of isolating interactant and selective vulcanization provides new ideas for effectively constructing heterostructure materials for lithium-sulfur batteries.

1. Introduction

With the utilization of renewable energy and the development of electric vehicles, electrochemical energy storage technology is facing great challenges including large specific capacity and fast charge–discharge rate.[1,2] Because of the high energy density and efficiency, lithium-ion batteries (LIBs) have become the main power source for abundant energy storage devices.[3–5] Since conventional LIBs have come close to their theoretical capacity, it is necessary to develop electrochemical batteries beyond the Li^+ intercalation mechanism to match the increasing energy storage demand. Recently, lithium-sulfur batteries (LSBs) have been

* Corresponding authors.
E-mail addresses: wangn@buaa.edu.cn (N. Wang), baowang@ipe.ac.cn (B. Wang), zhaoyong@buaa.edu.cn (Y. Zhao).

https://doi.org/10.1016/j.jcis.2021.08.171
0021-9797/

deemed as a potential choice to substitute traditional LIBs owing to their low cost, high theoretical energy density (2600 Wh kg^{-1}), and high theoretical specific capacity (~1675 mAh g^{-1}).[6–8] However, the large-scale application of LSBs is also constrained by many factors, mainly including the insulating nature of active material sulfur, the "shuttle effect" of polysulfides, and the sluggish electrode dynamics.[9,10]

Over the past decades, many researchers have been dedicated to addressing the aforementioned issues of LSBs such as preparing cathode and inter-layer materials with different structures,[11,12] optimizing electrolyte compositions,[13] and exploring new strategies for anode protection.[14] Among these methods, the reasonable designing of cathode host materials plays an important role in realizing high-efficiency electrochemistry reactions[15]. In general, the following aspects need to be considered according to the specificity of LSBs. (1) The active material sulfur has the characteristics of ionic and electronic insulation, which hinders the redox reaction during the charge–discharge process. So, a pass-through system should be established to rapidly conduct electrons and ions within the cathode. At present, the popular method is to use carbonaceous materials (such as carbon nanotubes,[16,17] graphene,[18] carbon nanofibers,[19,20] etc.) or metal compounds (such as TiN,[21,22] CoS_2,[23,24] TiO_{2-x},[25–27] etc.); (2) In the charge–discharge process, polysulfides (Li_2S_8, Li_2S_6, Li_2S_4, etc.) are generated which is highly soluble in the electrolyte. They lead to serious sulfur loss under the action of electric field or concentration gradient, namely "shuttle effect". To solve this problem, well-designed electrode structures (such as core–shell structure,[28,29] hollow structure,[30,31] multi-shell structure,[27] etc.) or polar material with intrinsic sulfiphilic property (such as metallic oxide,[32–34] metal sulfide,[35–37] metal nitride,[6,21,38] metal carbide,[39–41] etc.) can effectively confine polysulfides inside the cathode, thereby inhibiting shuttle effect and improving energy efficiency; (3) The entire LSBs charging and discharging process undergoes a series of electrochemical reactions, and produces a variety of intermediate products. Introducing new components (such as CoN_4,[42] MoS_2,[43] CoS_2,[23,44] etc.) to promote polysulfides redox is another solution to alleviate shuttle effect. Development of high-efficiency electrode materials that can increase conductivity, limit polysulfides diffusion, and promote polysulfides redoxs is a promising way to alleviate shuttle effect.

Now, many researchers adopt a strategy that combines materials with multi-structures and catalytic components to improve the electrochemical performance of LSBs.[35,45] Lou *et al.* designed carbon nanofibers filled with TiO hollow nanospheres,[46] which have nanoscale reaction chambers and conductive networks, showing excellent charge–discharge properties. Mai *et al.* reported a nitrogen-doped graphene/TiN nanocomposite that plays important roles in electron conduction and anchoring polysulfides[47]. Among multi-structures, the porous core–shell structure can store the active material while effectively confining the polysulfides; while among the catalytic components, CoS_2 has strong electrical conductivity to promote rapid electron transfer. The combination of them is an effective way to improve the electrochemical performance of LSBs.

In this work, we developed CoS_2-TiO_2@C core–shell fibers through coaxial electrospinning technique and selective vulcanization. The combination of core–shell structure and polar CoS_2 with catalytic effect results in strong confinement and faster redox rate to polysulfides, which effectively suppress shuttle effects. Consequently, the S-CoS_2-TiO_2@C electrodes show favorable electrochemical performance with the initial specific capacity of 1181.1 mAh g^{-1}, high rate capability up to 3C, and outstanding cyclability with a low capacity fading rate of 0.06% per cycle after 300 cycles. This strategy of isolating interactant and selective vulcanization provides new ideas for effectively constructing heterostructure materials for high-efficiency LSBs.

2. Results and discussion

We developed CoS_2-TiO_2@C core–shell electrode materials through coaxial electrospinning technique and selective vulcanization strategy. The synthetic process of S-CoS_2-TiO_2@C electrode has been illustrated in Fig. 1**a** and **Figure S1**. The ZIF-67 cubic nanoparticles (NPs) with uniform size (~250 nm) were firstly prepared (**Figure S2a**) as previously reported.[48] The crystallinity of ZIF-67 NPs was confirmed through the representative sharp peaks in the XRD pattern which are consistent with previous literature (Figure S2b).[49] Then, the ZIF-67 NPs were dispersed in solution of polystyrene (PS) / dimethyl formamide (DMF) as core fluid; polyvinyl pyrrolidone (PVP) was added to DMF with tetrabutyl titanate (TBOT) as shell fluid. The core–shell fibers were fabricated through coaxial electrospinning technology.[50] The precursor fibers with uniform diameter (~2.5 μm) show smooth surface and ZIF-67 NPs embedded inside the fiber, demonstrating a core–shell structure (Fig. 2**a and b**). After thermal treatment, the diameter of the fiber decreases, which is the result of polymer pyrolysis at high temperature. The CoS_2-TiO_2@C fibers have rough surfaces and abundant pores as shown in Fig. 2c and d. For comparison, we also prepared CoO-TiO_2@C core–shell fibers and TiO_2@C solid fibers (**Figure S3**). CoS_2-TiO_2@C fibers have many advantages when used as cathode host material: the highly porous core can effectively store sulfur; the carbon-containing shell provides fast short-range charge transfer; CoS_2 can facilitate the conversion of polysulfides.

The crystalline structures of the components in CoS_2-TiO_2@C (Fig. 3**a**) and CoO-TiO_2@C (**Figure S4a**) were investigated by XRD measurements. The diffraction peaks of both CoS_2 and TiO_2 are detected and indexed in the CoS_2-TiO_2@C fibers. To further investigate the carbon component of CoS_2-TiO_2@C and CoO-TiO_2@C, Raman characterization is presented in Fig. 3b. Two peaks located at 1344 and 1581 cm^{-1} were observed, which represent the

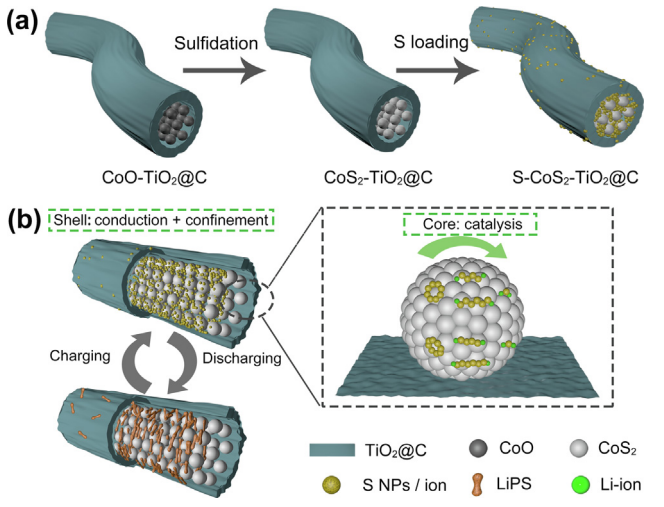

Fig. 1. (a) Schematic illustration for the preparation of S-CoS_2-TiO_2@C electrode materials. Firstly, CoO-TiO_2@C core–shell fibers are obtained through coaxial electrospinning, peroxidation, and carbonization. Then, CoS_2-TiO_2@C are obtained via sulfuration under Ar atmosphere. Finally, the S-CoS_2-TiO_2@C electrode is obtained by loading S (b) The S-CoS_2-TiO_2@C electrode in charge–discharge processes. Porous core–shell structure provides space for loading of active substances; Carbonaceous materials realize rapid electron conduction; TiO_2 enhances the chemisorption of polysulfides on the electrode material; CoS_2 promotes the redox reaction of intermediates.

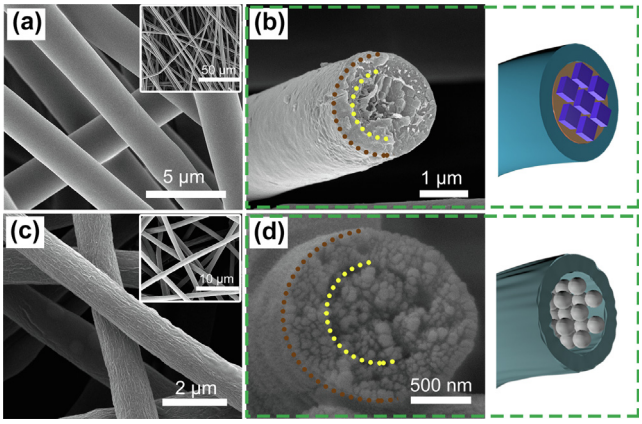

Fig. 2. (a) SEM images of the precursor fibers with the uniform diameter (~2.5 μm) and smooth surface. (b) Cross-sectional SEM image and core–shell structure schematic diagram of the precursor fiber, where ZIF-67 cubic nanoparticles were completely embedded in the fibers. (c) SEM images of CoS_2-TiO_2@C fibers with uniform diameter (~1.5 μm) and coarse surface after calcination. (d) Cross-sectional SEM image and core–shell structure schematic diagram of the CoS_2-TiO_2@C fiber, showing highly porous core for accommodating and confining active material.

disorder-induced vibrational mode (D band) and the symmetry-allowed vibrational feature (G band), respectively.[51] The low-intensity ratio (I_D / I_G) of the D band to G band indicates the presence of graphitic carbon components in the CoS_2-TiO_2@C and CoO-TiO_2@C fibers. The graphitic carbon can offer favorable electron conduction for a fast electrochemical reaction. Then the porous structure of the CoS_2-TiO_2@C fibers was studied via N_2 adsorption–desorption test (Fig. 3c and Figure S4b). The isotherm displays type-IV hysteresis that consists of micropores and mesopores, which is attributed to the thermal reaction of PVP and ZIF-67. The BET surface area of CoS_2-TiO_2@C fibers is 44.6 m^2 g^{-1}, and the porous size distribution shows peaks at 4.4 nm. The abundant pore structures of CoS_2-TiO_2@C provide a strong physical confinement effect to the active material, while the high surface area can form a rich electrode/electrolyte interface for effective multiphase interface reaction.[52]

The surface composition of CoS_2-TiO_2@C was studied via XPS. The high-resolution spectrum of C1s displays three subpeaks, as shown in Fig. 3d. The two subpeaks located at 285.8 and 287.3 eV are corresponding to the bonds of C=N and C—N, respectively, which demonstrate the *N*-doping of the carbon matrix. The chemical status was further investigated by N1s high-resolution spectra (Fig. 3e). The aforementioned spectrum was differentiated into three subpeaks of pyridinic N (398.1 eV), pyrrolic N (399.4 eV), and graphitic N (401.1 eV).[11,53] The *N*-doping increases the polarity of the carbon matrix to effectively anchor polysulfides and favor the redox reactions. Besides, TGA was employed to calculate the sulfur content in the electrode of S-CoS_2-TiO_2@C and S-CoO-TiO_2@C. As shown in Fig. 3f, the samples display continuous weight loss from 190 to 400 °C in N_2 environment. The S-CoO-TiO_2@C and S-CoS_2-TiO_2@C present weight loss of ~ 63.3% and ~ 66.3%, respectively, which can accurately calculate the sulfur content in the electrode.

Considering the advantage of core–shell structure and composite composition, CoS_2-TiO_2@C fibers were applied as cathode host material for LSBs. The CV curves show two typical pairs of sulfur redox peaks from 1.7–2.8 V (Fig. 4**a**). As seen, the S-CoS_2-TiO_2@C electrodes deliver higher redox current peak and smaller redox potential gaps than the S-CoO-TiO_2@C electrode, which indicates the facilitated redox reactions in the S-CoS_2-TiO_2@C electrodes. Besides, to clarify the contribution of capacity, CV curve of the sulfur-free electrode was tested in the potential range of 1.7–2.8 V that the sulfur-free electrode has no obvious redox peak (**Figure S5a**). It proves that all capacity comes from the electrochemical reaction of S. The performance evaluation of the S-CoS_2-TiO_2@C and S-CoO-TiO_2@C electrodes was tested by galvanostatic charge–discharge. Fig. 4b shows the typical voltage profiles at a rate of 0.2C. Both electrodes exhibit the typical two discharge plateaus corresponding to the electrochemical reduction process of S. The first discharge plateau (~2.3 V) corresponds to the transformation from solid sulfur (S_8) to soluble polysulfides (Li_2S_n, $8 \geq n \geq 4$). The second discharge plateau (~2.1 V) corresponds to the transformation of insoluble Li_2S_2 and Li_2S through the further electrochemical reduction process of the polysulfides. The S-CoS_2-TiO_2@C electrode deliver initial specific capacity of 1181.1 mAh g^{-1}, which is 70.5% of its theoretical limit and higher than that of the S-CoO-

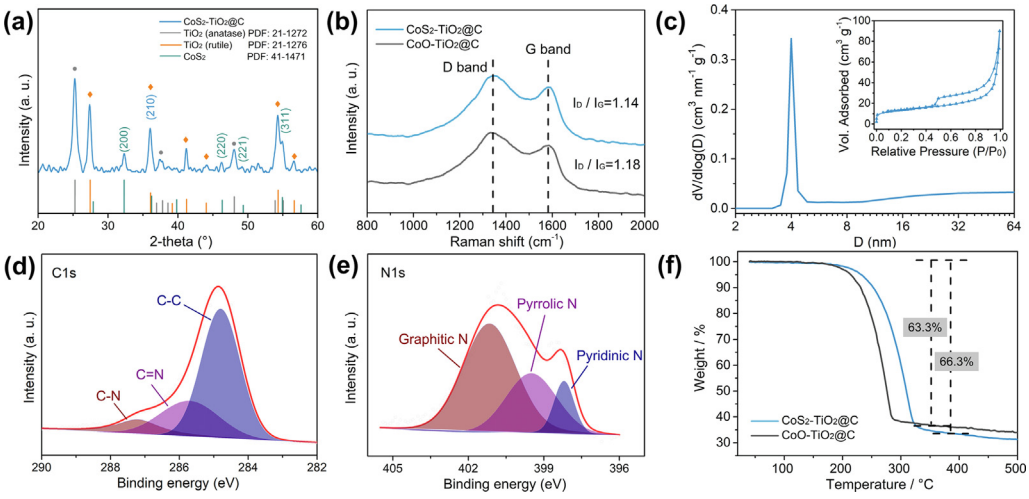

Fig. 3. (a) XRD pattern of CoS_2-TiO_2@C fibers, showing diffraction peaks of each component of CoS_2-TiO_2@C. (b) Raman spectra of the CoS_2-TiO_2@C and CoO-TiO_2@C fibers. The low-intensity ratio (I_D / I_G) of the D band to G band indicates the presence of graphitic carbon components. (c) Pore distribution and N_2 adsorption–desorption isotherm curve (inset) of the CoS_2-TiO_2@C fibers. The isotherm displays type-IV hysteresis that consists of micropores and mesopores, which is attributed to the thermal reaction of PVP and ZIF-67. (d) High-resolution XPS spectra of C1s for the CoS_2-TiO_2@C fibers. The two subpeaks located at 285.8 and 287.3 eV are corresponding to the bonds of C=N and C—N, respectively. (e) N1s of the CoS_2-TiO_2@C fibers shows three subpeaks of pyridinic N (398.1 eV), pyrrolic N (399.4 eV), and graphitic N (401.1 eV). (f) TGA of the S-CoS_2-TiO_2@C and S-CoO-TiO_2@C present weight loss of ~ 66.3% and ~ 63.3%, respectively.

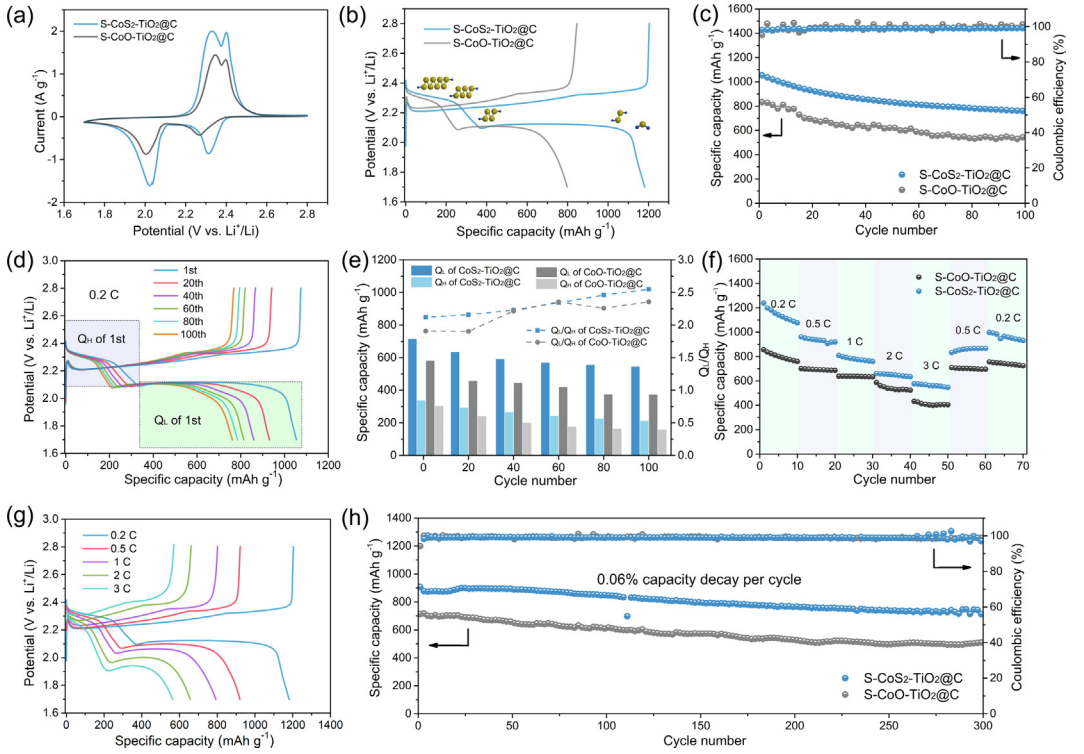

Fig. 4. Electrochemical characterization of S-CoS_2-TiO_2@C and S-CoO-TiO_2@C electrodes. (a) CV curves at a rate of 0.1 mV s^{-1} showing two typical pairs of sulfur redox peaks from 1.7 – 2.8 V. (b) Charge-discharge profiles at a rate of 0.2C. The S-CoS_2-TiO_2@C electrodes deliver initial specific capacity of 1181.1 mAh g^{-1}, which is higher than that of the S-CoO-TiO_2@C electrodes (832.7 mAh g^{-1}). (c) Cycling performances at 0.2C. (d) Charge-discharge profiles of S-CoS_2-TiO_2@C electrodes at 0.2C. The S-CoS_2-TiO_2@C electrodes show higher capacity and better cycling stability. (e) The capacities of high (Q_H) and low (Q_L) plateau of S-CoS_2-TiO_2@C and S-CoO-TiO_2@C at different cycles (column). The Q_H/Q_L of S-CoS_2-TiO_2@C and S-CoO-TiO_2@C electrodes at 0.2C (dotline). The S-CoS_2-TiO_2@C electrodes deliver higher Q_H and Q_L than the S-CoO-TiO_2@C electrode, indicating that the S-CoS_2-TiO_2@C electrodes can block and effectively utilize polysulfides. (f) Specific discharging capacities at different rates. (g) The charge–discharge profiles at various rates. The S-CoS_2-TiO_2@C electrodes exhibit high capabilities (1181.1, 919.7, 792.5, 656.7, and 563.0 mAh g^{-1} at the rate of 0.2, 0.5, 1, 2, and 3C, respectively). (h) Long-term cycling performance at a rate of 1C. The S-CoS_2-TiO_2@C electrodes deliver a high capacity of 736.5 mAh g^{-1} after 300 cycles with high coulombic efficiency over 99.5% (capacity decay of only 0.06% per cycle).

TiO_2@C electrode (832.7 mAh g^{-1}), showing an enhanced utilization of sulfur in the S-CoS_2-TiO_2@C and S-TiO_2@C electrodes (**Figure S6**). This is attributed to the combination of core–shell structure and composite composition, resulting in strong confinements and conversion for polysulfides. Fig. 4c shows the cycling performances of S-CoS_2-TiO_2@C and S-CoO-TiO_2@C electrodes that the S-CoS_2-TiO_2@C electrode shows higher capacity and better cycling stability with a higher capacity retention of 72.1% after 100 cycles at a rate of 0.2C, while the S-CoO-TiO_2@C electrodes retain only 65.7% of their initial capacities. Fig. 4d displays the charge–discharge profiles of the S-CoS_2-TiO_2@C electrodes at 0.2C. The two typical voltage plateaus still overlap even after 100 cycles, which proves that the S-CoS_2-TiO_2@C electrodes can restrict "shuttle effects" and enhance the reversibility of electrochemical reaction. As shown in Fig. 4e and S5b, S-CoS_2-TiO_2@C electrode can deliver higher Q_H and Q_L than the S-CoO-TiO_2@C electrode, indicating that the S-CoS_2-TiO_2@C electrodes can effectively block and utilize polysulfides. Furthermore, higher Q_L/Q_H of the battery with S-CoS_2-TiO_2@C electrodes suggests that the conductive and polar CoS_2can promote the reduction of polysulfides. The rate capabilities were evaluated as shown in Fig. 4f. The S-CoS_2-TiO_2@C electrode exhibits better capabilities (1181.1, 919.7, 792.5, 656.7, and 563.0 mAh g^{-1} at rate of 0.2, 0.5, 1, 2, and 3C, respectively) than the S-CoO-TiO_2@C electrode. In Fig. 4g, the two typical voltage plateaus of S-CoS_2-TiO_2@C electrodes can slightly offset to low voltage and keep stable at different current densities, indicating the excellent conductivity of S-CoO-TiO_2@C electrodes. Moreover, long cycle performance of the S-CoS_2-TiO_2@C and S-CoO-TiO_2@C electrodes was investigated at a rate of 1C as shown in Fig. 4h. The S-CoS_2-TiO_2@C electrodes delivers a high capacity of 736.5 mAh g^{-1} after 300 cycles with high coulombic efficiency over 99.5% (capacity decay of only 0.06% per cycle). In contrast, the S-CoO-TiO_2@C electrodes display 510.9 mAh g^{-1} over 300 cycles. Due to the core–shell structure and catalytic properties of the components, the S-CoO-TiO_2@C electrode shows better availability of active substances, rate performance and cycling stability.

To verify the chemical adsorption abilities, polysulfides adsorption tests of CoS_2-TiO_2@C and CoO-TiO_2@C were performed. After being aged for 5 h, the CoS_2-TiO_2@C faded more obvious than that of the CoO-TiO_2@C (Fig. 5**a**), indicating that CoS_2-TiO_2@C can offer strong chemical anchoring for polysulfides. Ultraviolet–visible (UV) absorption measurements show that the adsorption peak after 5 h of CoS_2-TiO_2@C is weaker than CoO-TiO_2@C, implying CoS_2 enhances the adsorption properties of electrode material to polysulfides. As shown in Fig. 5b, before interacting with Li_2S_8 solution, the Co $2p_{3/2}$ is consisted of Co^{2+} at 781.8 eV and traces Co^{3+} at 778.8 eV.[54] After interacting with Li_2S_8 solution, the Co-ion peaks shift to lower binding energy, which is attributed to the strong chemical affinity between polysulfides and Co-ion.[55] This chemical interaction contributes to adsorb and catalyze soluble polysulfides on the CoS_2 surface, which brings a good cycling performance for LSBs to a great extent.[56,57] To study the electrochemical kinetics, electrochemical impedance spectroscopy (EIS) was performed on S-CoS_2-TiO_2@C, S-CoO-TiO_2@C (Fig. 5c), and S-TiO_2@C electrodes (**Figure S7**). The S-CoS_2-TiO_2@C electrode shows smaller charge-transfer resistance (~41.9 Ω) than the S-CoO-TiO_2@C electrode (~51.6 Ω), indicating that the introduction of

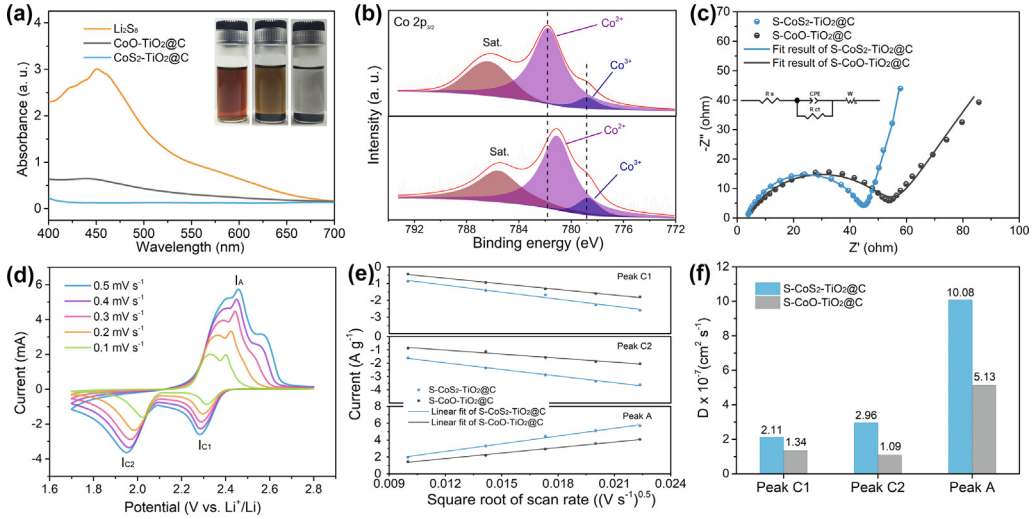

Fig. 5. (a) UV spectrum of Li_2S_8 solution and solutions after the adsorption test. The inset is the photo of Li_2S_8 solution (left), Li_2S_8 solution with CoO-TiO_2@C (middle) and CoS_2-TiO_2@C (right) after being aged for 5 h. The adsorption peaks after adding CoS_2-TiO_2@C is weaker than CoO-TiO_2@C, implying the polysulfides adsorption is improved by CoS_2. (b) XPS spectra of the pristine CoS_2-TiO_2@C and precipitate recovered from Li_2S_8/CoS_2-TiO_2@C suspension. The shift of binding energy is attributed to the strong chemical affinity between polysulfides and Co-ion. (c) Nyquist plots of S-CoS_2-TiO_2@C and S-CoO-TiO_2@C electrodes from 10 MHz to 100 mHz. The inset is the equivalent circuit model. The S-CoS_2-TiO_2@C electrode shows smaller charge-transfer resistance (~41.9 Ω) than the S-CoO-TiO_2@C electrode (~51.6 Ω), indicating that the introduction of CoS_2 can reduce the internal resistance. (d) CV curves of S-CoS_2-TiO_2@C at different scan rates. (e) The relationship between the peak current and square root of the scan rate in the S-CoS_2-TiO_2@C and S-CoO-TiO_2@C electrodes. (f) The Li^+ diffusion coefficient of S-CoS_2-TiO_2@C and S-CoO-TiO_2@C electrodes. The higher values of S-CoS_2-TiO_2@C electrodes imply the excellent Li^+ diffusion rate in charge–discharge processes.

CoS_2 can reduce the internal resistance. The smaller charge-transfer resistance contributes to a faster charge transfer rate and electrochemical kinetics.[58] The chemical diffusion coefficient of Li^+ was also studied by using CV curves at different scanning rates. Fig. 5d and **Figure S8** show the CV curves of the S-CoS_2-TiO_2@C, S-CoO-TiO_2@C, and S-TiO_2@C electrodes. It can be clearly observed that the cathodic peaks shift to lower potentials, the anodic peaks shift to higher potentials with increase of scan rate. In fact, the peak currents (I_p) of redox process are also proportional to the square root of scan rate (Fig. 5e). Furthermore, the property of L diffusivity was analyzed by the CV of the S-CoS_2-TiO_2@C and S-CoO-TiO_2@C electrodes. In sulfur redox processes, Li^+ diffusion coefficient (D) can be described by the Randles-Sevcik equation: [59]

$$I_p = \left(2.69 \times 10^5\right) n^{1.5} S\, D^{0.5} \Delta C\, v^{0.5}$$

Where I_p is the peak current, n is the number of transferred electrons, S represents the electrode area, D represents the Li^+ diffusion coefficient, ΔC represents the change of Li^+ concentration, v represents the CV scan rate. As shown in Fig. 5f, the S-CoS_2-TiO_2@C electrode exhibits excellent Li^+ diffusion coefficient during three redox peaks, indicating that CoS_2-TiO_2@C can promote the conversion of polysulfides and increase the electrochemical reaction rate. [59] Additionally, the S-CoS_2-TiO_2@C electrodes also show smaller potential gaps in charge–discharge processes, while the CV curve delivers smaller redox potential gaps (**Figure S9**). These results clearly indicate the facilitated S redox reactions by the S-CoS_2-TiO_2@C electrodes. Compared with S-CoO-TiO_2@C electrode, S-CoS_2-TiO_2@C shows better electrochemical performance because of the stronger adsorption capacity for polysulfides, smaller charge-transfer resistance, and faster redox rate.

To further evaluate the catalytic effect of cathode host materials in LSBs, the CV curves in symmetric cells were performed as shown in Fig. 6**a** and **Figure S10**. It can be clearly observed that the symmetric cells with Li_2S_6 both display intensive current response, while no redox peaks are observed in the cells without Li_2S_6, which supports the previous experimental results (Figure S5). The symmetrical cells of CoS_2-TiO_2@C cathode host materials show higher peak currents, which can be identified by the distinct peaks (−0.62, −0.12, 0.12, and 0.64 V), demonstrating the enhanced catalytic performance for polysulfide.[60–63] This intensive current

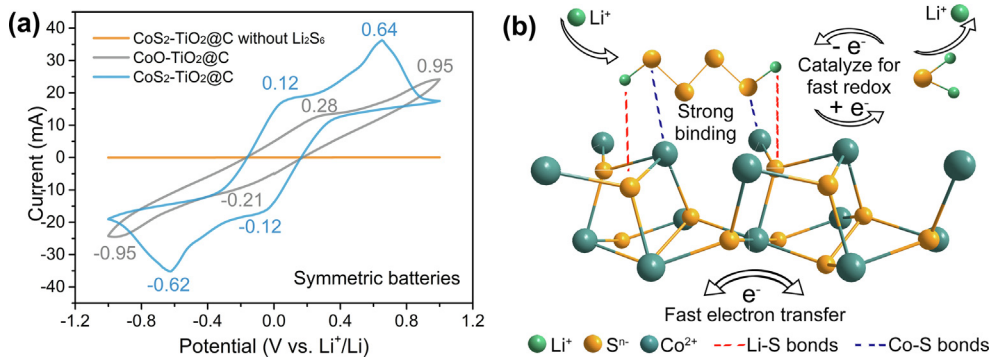

Fig. 6. (a) CV curves of the symmetric cells at a scan rate of 5 mV s^{-1} that the CoS_2-TiO_2@C electrodes display intensive current response. (b) Schematic processes of the polysulfides adsorption and conversion on CoS_2 interface. The polysulfides form Li-S and Co-S bonds and transform rapidly between solid and liquid phases at CoS_2 interface.

response indicates that the reactions of active materials dominate the current response instead of double-layer capacitance.[59] The (200), (210), (220), (221), and (311) planes are revealed in XRD patterns (Fig. 3a). The adsorption and conversion process of polysulfides on CoS_2 interface can be illustrated in Fig. 6**b** and Figure S11 by taking (200) plane as an example. During charging and discharging, the soluble polysulfides are anchored by forming Li-S and Co-S bonds at CoS_2 interface. Under the catalytic effect and high conductivity of CoS_2, these polysulfides will gain and lose electrons and transform between the solid and liquid phases, rapidly. This makes the S-CoS_2-TiO_2@C electrode with good electrochemical properties.

3. Conclusions

CoS_2-TiO_2@C core–shell fibers have been designed and fabricated by combination of coaxial electrospinning and heat vulcanization treatments. The CoS_2 nanoparticles were wrapped by *N*-doped carbon layer and polar TiO_2, which realizes the functions of enhancing adsorption capacity for polysulfides, reducing charge-transfer resistance, and facilitating sulfur redox reactions. Consequently, the CoS_2-TiO_2@C core–shell fibers realize an outstanding electrochemical performance, *i.e.*, higher initial capacity of 1181.1 mAh g^{-1}, high rate capability up to 3C, and excellent cyclability with a low fading rate of 0.06% per cycle after 300 cycles. This study gives an effective way to solve the obstacles for high-performance sulfur electrode materials. This structure design can also be extended to fabricate multifunctional material in other energy storage and electrochemical catalysis applications.

CRediT authorship contribution statement

Dianming Li: Data curation, Writing – original draft. **Hongtai Li:** Software, Validation. **Shumin Zheng:** Software, Validation. **Ning Gao:** Software, Validation. **Shuai Li:** Visualization, Investigation. **Jing Liu:** Visualization, Investigation. **Lanlan Hou:** Visualization, Investigation. **Jingchong Liu:** Visualization, Investigation. **Beibei Miao:** Visualization, Investigation. **Jie Bai:** Conceptualization, Writing - review & editing. **Nü Wang:** Conceptualization, Writing - review & editing. **Bao Wang:** Conceptualization, Writing - review & editing. **Yong Zhao:** Conceptualization, Writing - review & editing.

Declaration of Competing Interest

The authors declare that they have no known competing financial interests or personal relationships that could have appeared to influence the work reported in this paper.

Acknowledgments

The authors acknowledge the National Natural Science Foundation of China (NSFC) (Grant Nos. 21975007, 21774005, 21433012, and 51772010), the National Natural Science Foundation for Outstanding Youth Foundation, the Fundamental Research Funds for the Central Universities, the National Program for Support of Top-notch Young Professionals, and the 111 project (Grant No. B14009).

Appendix A. Supplementary data

Supplementary data to this article can be found online at https://doi.org/10.1016/j.jcis.2021.08.171.

References

[1] Z.W. Seh, Y. Sun, Q. Zhang, Y. Cui, Designing High-Energy Lithium-Sulfur Batteries, Chem. Soc. Rev. 45 (2016) 5605, https://doi.org/10.1039/c5cs00410a.
[2] B. Scrosati, J. Hassoun, Y.K. Sun, Lithium-Ion Batteries A Look into the Future, Energy Environ. Sci. 4 (2011) 3287, https://doi.org/10.1039/c1ee01388b.
[3] S. Xie, H. Wang, T. Yao, J. Wang, C. Wang, J.W. Shi, X. Han, T. Liu, Y. Cheng, Embedding Comoo4 Nanoparticles into Porous Electrospun Carbon Nanofibers Towards Superior Lithium Storage Performance, J. Colloid Interface Sci. 553 (2019) 320, https://doi.org/10.1016/j.jcis.2019.06.039.
[4] M. Watanabe, M.L. Thomas, S. Zhang, K. Ueno, T. Yasuda, K. Dokko, Application of Ionic Liquids to Energy Storage and Conversion Materials and Devices, Chem. Rev. 117 (2017) 7190, https://doi.org/10.1021/acs.chemrev.6b00504.
[5] L. Ma, B. Hou, N. Shang, S. Zhang, C. Wang, L. Zong, J. Song, J. Wang, X. Zhao, The Precise Synthesis of Twin-Born Fe_3O_4/FeS/Carbon Nanosheets for High-Rate Lithium-Ion Batteries, Materials Chemistry, Frontiers (2021), https://doi.org/10.1039/D1QM00153A.
[6] N. Mosavati, V.R. Chitturi, S.O. Salley, K.Y.S. Ng, Nanostructured Titanium Nitride as a Novel Cathode for High Performance Lithium/Dissolved Polysulfide Batteries, J. Power Sources 321 (2016) 87, https://doi.org/10.1016/j.jpowsour.2016.04.099.
[7] A. Manthiram, S.H. Chung, C. Zu, Lithium-Sulfur Batteries: Progress and Prospects, Adv. Mater. 27 (2015) 1980, https://doi.org/10.1002/adma.201405115.
[8] Y.K. Sun, C.S. Yoon, Growing Instead of Confining, Nat. Energy 2 (2017) 768, https://doi.org/10.1038/s41560-017-0008-9.
[9] M. Faheem, W. Li, N. Ahmad, L. Yang, M.K. Tufail, Y. Zhou, L. Zhou, R. Chen, W. Yang, Chickpea Derived Co Nanocrystal Encapsulated in 3D Nitrogen-Doped Mesoporous Carbon: Pressure Cooking Synthetic Strategy and Its Application in Lithium-Sulfur Batteries, J. Colloid Interface Sci. 585 (2020) 328, https://doi.org/10.1016/j.jcis.2020.11.050.
[10] J. Wang, J. Li, Cobalt-Based Zeolitic Imidazolate Frameworks Modified Separator as Efficient Polysulfide Adsorbent for High Performance Lithium-Sulfur Batteries, J. Colloid Interface Sci. 584 (2020) 354, https://doi.org/10.1016/j.jcis.2020.10.009.
[11] Y. Qiu, L. Fan, M. Wang, X. Yin, X. Wu, X. Sun, D. Tian, B. Guan, D. Tang, N. Zhang, Precise Synthesis of Fe-N_2 Sites with High Activity and Stability for Long-Life Lithium-Sulfur Batteries, ACS Nano 14 (2020) 16105, https://doi.org/10.1021/acsnano.0c08056.
[12] B. Hao, H. Li, W. Lv, Y. Zhang, S. Niu, Q. Qi, S. Xiao, J. Li, F. Kang, Q.-H. Yang, Reviving Catalytic Activity of Nitrides by the Doping of the Inert Surface Layer to Promote Polysulfide Conversion in Lithium-Sulfur Batteries, Nano Energy 60 (2019) 305, https://doi.org/10.1016/j.nanoen.2019.03.064.
[13] F. Wu, F. Chu, G.A. Ferrero, M. Sevilla, A.B. Fuertes, O. Borodin, Y. Yu, G. Yushin, Boosting High-Performance in Lithium-Sulfur Batteries Via Dilute Electrolyte, Nano Lett. 20 (2020) 5391, https://doi.org/10.1021/acs.nanolett.0c01778.
[14] H. Zhao, N. Deng, J. Yan, W. Kang, J. Ju, Y. Ruan, X. Wang, X. Zhuang, Q. Li, B. Cheng, A Review on Anode for Lithium-Sulfur Batteries: Progress and Prospects, Chem. Eng. J. 347 (2018) 343, https://doi.org/10.1016/j.cej.2018.04.112.
[15] A. Fu, C. Wang, F. Pei, J. Cui, X. Fang, N. Zheng, Recent Advances in Hollow Porous Carbon Materials for Lithium-Sulfur Batteries, Small 15 (2019), https://doi.org/10.1002/smll.201804786 e1804786.
[16] L. Yang, G. Li, X. Jiang, T. Zhang, H. Lin, J.Y. Lee, Balancing the Chemisorption and Charge Transport Properties of the Interlayer in Lithium-Sulfur Batteries, J. Mater. Chem. A 5 (2017) 12506, https://doi.org/10.1039/c7ta01352c.
[17] Y.S. Su, Y. Fu, A. Manthiram, Self-Weaving Sulfur-Carbon Composite Cathodes for High Rate Lithium-Sulfur Batteries, Phys. Chem. Chem. Phys. 14 (2012) 14495, https://doi.org/10.1039/c2cp42796f.
[18] F. Wu, S. Zhao, J. Li, Y. Lu, Y. Su, L. Chen, L. Bao, J. Yao, X. Liu, Hand-in-Hand Reinforced rGO Film Used as an Auxiliary Functional Layer for High-Performance Li-S Batteries, ACS Appl. Mater. Interfaces 11 (2019) 12544, https://doi.org/10.1021/acsami.9b00845.
[19] Z. Li, J.T. Zhang, Y.M. Chen, J. Li, X.W. Lou, Pie-Like Electrode Design for High-Energy Density Lithium-Sulfur Batteries, Nat. Commun. 6 (2015) 8850, https://doi.org/10.1038/ncomms9850.
[20] J.S. Lee, W. Kim, J. Jang, A. Manthiram, Sulfur-Embedded Activated Multichannel Carbon Nanofiber Composites for Long-Life High-Rate Lithium-Sulfur Batteries, Adv. Energy Mater. 7 (2017), https://doi.org/10.1002/aenm.201601943 1601943.
[21] Y. Yao, H. Wang, H. Yang, S. Zeng, R. Xu, F. Liu, P. Shi, Y. Feng, K. Wang, W. Yang, X. Wu, W. Luo, Y. Yu, A Dual-Functional Conductive Framework Embedded with TiN-VN Heterostructures for Highly Efficient Polysulfide and Lithium Regulation toward Stable Li-S Full Batteries, Adv. Mater. 32 (2020), https://doi.org/10.1002/adma.201905658 e1905658.
[22] Y. Liao, J. Xiang, L. Yuan, Z. Hao, J. Gu, X. Chen, K. Yuan, P.K. Kalambate, Y. Huang, Biomimetic Root-Like TiN/C@S Nanofiber as a Freestanding Cathode with High Sulfur Loading for Lithium-Sulfur Batteries, ACS Appl. Mater. Interfaces 10 (2018) 37955, https://doi.org/10.1021/acsami.8b11118.
[23] Z. Yuan, H.J. Peng, T.Z. Hou, J.Q. Huang, C.M. Chen, D.W. Wang, X.B. Cheng, F. Wei, Q. Zhang, Powering Lithium-Sulfur Battery Performance by Propelling Polysulfide Redox at Sulfiphilic Hosts, Nano Lett. 16 (2016) 519, https://doi.org/10.1021/acs.nanolett.5b04166.
[24] Q. Hu, J. Lu, C. Yang, C. Zhang, J. Hu, S. Chang, H. Dong, C. Wu, Y. Hong, L. Zhang, Promoting Reversible Redox Kinetics by Separator Architectures Based on

CoS_2/HPGC Interlayer as Efficient Polysulfide-Trapping Shield for Li-S Batteries, Small 16 (2020), https://doi.org/10.1002/smll.202002046 e2002046.
[25] H. Wei, E.F. Rodriguez, A.S. Best, A.F. Hollenkamp, D. Chen, R.A. Caruso, Chemical Bonding and Physical Trapping of Sulfur in Mesoporous Magneli Ti_4O_7 Microspheres for High- Performance Li-S Battery, Adv. Energy Mater. 7 (2017), https://doi.org/10.1002/aenm.201601616 1601616.
[26] S. Mei, C.J. Jafta, I. Lauermann, Q. Ran, M. Kaergell, M. Ballauff, Y. Lu, Porous Ti_4O_7 Particles with Interconnected-Pore Structure as a High-Efficiency Polysulfide Mediator for Lithium-Sulfur Batteries, Adv. Funct. Mater. 27 (2017), https://doi.org/10.1002/adfm.201701176 1701176.
[27] E.H.M. Salhabi, J. Zhao, J. Wang, M. Yang, B. Wang, D. Wang, Hollow Multi-Shelled Structural TiO_{2-X} with Multiple Spatial Confinement for Long-Life Lithium-Sulfur Batteries, Angew. Chem. Int. Ed. Engl. 58 (2019) 9078, https://doi.org/10.1002/anie.201903295.
[28] C. Zhao, G.L. Xu, T. Zhao, K. Amine, Beyond the Polysulfide Shuttle and Lithium Dendrite Formation: Addressing the Sluggish Sulfur Redox Kinetics for Practical High-Energy Li-S Batteries, Angew. Chem. Int. Ed. Engl. 59 (2020) 17634, https://doi.org/10.1002/anie.202007159.
[29] Q. Sun, B. He, X.Q. Zhang, A.H. Lu, Engineering of Hollow Core-Shell Interlinked Carbon Spheres for Highly Stable Lithium-Sulfur Batteries, ACS Nano 9 (2015) 8504, https://doi.org/10.1021/acsnano.5b03488.
[30] L. Yu, H. Hu, H.B. Wu, X.W. Lou, Complex Hollow Nanostructures: Synthesis and Energy-Related Applications, Adv. Mater. 29 (2017), https://doi.org/10.1002/adma.201604563 1604563.
[31] J.S. Lee, J. Jun, J. Jang, A. Manthiram, Sulfur-Immobilized, Activated Porous Carbon Nanotube Composite Based Cathodes for Lithium-Sulfur Batteries, Small 13 (2017), https://doi.org/10.1002/smll.201602984 1602984.
[32] D. Luo, Z. Zhang, G. Li, S. Cheng, S. Li, J. Li, R. Gao, M. Li, S. Sy, Y.P. Deng, Y. Jiang, Y. Zhu, H. Dou, Y. Hu, A. Yu, Z. Chen, Revealing the Rapid Electrocatalytic Behavior of Ultrafine Amorphous Defective Nb_2O_{5-X} Nanocluster toward Superior Li-S Performance, ACS Nano 14 (2020) 4849, https://doi.org/10.1021/acsnano.0c00799.
[33] Y. Tao, Y. Wei, Y. Liu, J. Wang, W. Qiao, L. Ling, D. Long, Kinetically-Enhanced Polysulfide Redox Reactions by Nb_2O_5 Nanocrystals for High-Rate Lithium-Sulfur Battery, Energy Environ. Sci. 9 (2016) 3230, https://doi.org/10.1039/c6ee01662f.
[34] S. Evers, T. Yim, L.F. Nazar, Understanding the Nature of Absorption/Adsorption in Nanoporous Polysulfide Sorbents for the Li-S Battery, J. Phys. Chem. C 116 (2012) 19653, https://doi.org/10.1021/jp304380j.
[35] H. Zhang, M. Zou, W. Zhao, Y. Wang, Y. Chen, Y. Wu, L. Dai, A. Cao, Highly Dispersed Catalytic Co_3S_4 among a Hierarchical Carbon Nanostructure for High-Rate and Long-Life Lithium-Sulfur Batteries, ACS Nano 13 (2019) 3982, https://doi.org/10.1021/acsnano.8b07843.
[36] A. Paolella, D. Laul, V. Timoshevskii, W. Zhu, S. Marras, G. Bertoni, A.S. Wahba, G. Girard, C. Gagnon, L. Rodrigue, B. Commarieu, A. Guerfi, R. Gauvin, M.L. Trudeau, A. Vijh, M. Armand, K. Zaghib, The Role of Metal Disulfide Interlayer in Li-S Batteries, J. Phys. Chem. C 122 (2018) 1014, https://doi.org/10.1021/acs.jpcc.7b08719.
[37] M. Choi, S.K. Koppala, D. Yoon, J. Hwang, S.M. Kim, J. Kim, A Route to Synthesis Molybdenum Disulfide-Reduced Graphene Oxide (MoS_2-rGO) Composites Using Supercritical Methanol and Their Enhanced Electrochemical Performance for Li-Ion Batteries, J Power Sources 309 (2016) 202, https://doi.org/10.1016/j.jpowsour.2016.01.081.
[38] Z. Shen, Z. Zhang, M. Li, Y. Yuan, Y. Zhao, S. Zhang, C. Zhong, J. Zhu, J. Lu, H. Zhang, Rational Design of a $Ni_3N_{0.85}$ Electrocatalyst to Accelerate Polysulfide Conversion in Lithium-Sulfur Batteries, ACS Nano 14 (2020) 6673, https://doi.org/10.1021/acsnano.9b09371.
[39] X. Li, Y. Zhang, S. Wang, Y. Liu, Y. Ding, G. He, N. Zhang, G. Yu, Hierarchically Porous C/Fe_3C Membranes with Fast Ion-Transporting Channels and Polysulfide-Trapping Networks for High-Areal-Capacity Li-S Batteries, Nano Lett. 20 (2020) 701, https://doi.org/10.1021/acs.nanolett.9b04551.
[40] F. Zhou, Z. Li, X. Luo, T. Wu, B. Jiang, L.L. Lu, H.B. Yao, M. Antonietti, S.H. Yu, Low Cost Metal Carbide Nanocrystals as Binding and Electrocatalytic Sites for High Performance Li-S Batteries, Nano Lett. 18 (2018) 1035, https://doi.org/10.1021/acs.nanolett.7b04505.
[41] A. Ghosh, M.S. Garapati, A.P.V.K. Saroja, R. Sundara, Polar Bilayer Cathode for Advanced Lithium-Sulfur Battery: Synergy between Polysulfide Conversion and Confinement, J. Phys. Chem. C 123 (2019) 10777, https://doi.org/10.1021/acs.jpcc.9b01371.
[42] K. Xiao, J. Wang, Z. Chen, Y. Qian, Z. Liu, L. Zhang, X. Chen, J. Liu, X. Fan, Z.X. Shen, Improving Polysulfides Adsorption and Redox Kinetics by the Co_4N Nanoparticle/N-Doped Carbon Composites for Lithium-Sulfur Batteries, Small 15 (2019), https://doi.org/10.1002/smll.201901454 e1901454.
[43] E. Cha, M.D. Patel, J. Park, J. Hwang, V. Prasad, K. Cho, W. Choi, 2D MoS_2 as an Efficient Protective Layer for Lithium Metal Anodes in High-Performance Li-S Batteries, Nat. Nanotechnol. 13 (2018) 337, https://doi.org/10.1038/s41565-018-0061-y.
[44] J. Zhang, Z. Li, X.W.D. Lou, A Freestanding Selenium Disulfide Cathode Based on Cobalt Disulfide-Decorated Multichannel Carbon Fibers with Enhanced Lithium Storage Performance, Angew. Chem. Int. Ed. Engl. 56 (2017) 14107, https://doi.org/10.1002/anie.201708105.
[45] Z. Li, Z. Xiao, P. Li, X. Meng, R. Wang, Enhanced Chemisorption and Catalytic Effects toward Polysulfides by Modulating Hollow Nanoarchitectures for Long-Life Lithium-Sulfur Batteries, Small 16 (2020), https://doi.org/10.1002/smll.201906114 e1906114.
[46] Z. Li, B.Y. Guan, J. Zhang, X.W. Lou, A Compact Nanoconfined Sulfur Cathode for High-Performance Lithium-Sulfur Batteries, Joule 1 (2017) 576, https://doi.org/10.1016/j.joule.2017.06.003.
[47] Z. Li, Q. He, X. Xu, Y. Zhao, X. Liu, C. Zhou, D. Ai, L. Xia, L. Mai, A 3D Nitrogen-Doped Graphene/TiN Nanowires Composite as a Strong Polysulfide Anchor for Lithium-Sulfur Batteries with Enhanced Rate Performance and High Areal Capacity, Adv. Mater. 30 (2018), https://doi.org/10.1002/adma.201804089 e1804089.
[48] H. Hu, B.Y. Guan, X.W. Lou, Construction of Complex CoS Hollow Structures with Enhanced Electrochemical Properties for Hybrid Supercapacitors, Chem 1 (2016) 102, https://doi.org/10.1016/j.chempr.2016.06.001.
[49] G. Li, W. Lei, D. Luo, Y. Deng, Z. Deng, D. Wang, A. Yu, Z. Chen, Stringed "Tube on Cube" Nanohybrids as Compact Cathode Matrix for High-Loading and Lean-Electrolyte Lithium-Sulfur Batteries, Energy Environ. Sci. 11 (2018) 2372, https://doi.org/10.1039/c8ee01377b.
[50] D. Li, F. Guo, Z. Cui, J. Zhou, Y. Zhai, Y. Du, J. Liu, N. Wang, Y. Zhao, Controllable and Continuous Hollow Fiber Swimmers Based on the Marangoni Effect, ACS Appl. Mater. Interfaces 12 (2020) 53503, https://doi.org/10.1021/acsami.0c15764.
[51] H. Li, Q. Jin, D. Li, X. Huan, Y. Liu, G. Feng, J. Zhao, W. Yang, Z. Wu, B. Zhong, X. Guo, B. Wang, Mo_2C-Embedded Carambola-Like N, S-Rich Carbon Framework as the Interlayer Material for High-Rate Lithium-Sulfur Batteries in a Wide Temperature Range, ACS Appl. Mater. Interfaces 12 (2020) 22971, https://doi.org/10.1021/acsami.0c04842.
[52] M. Wang, X. Xia, Y. Zhong, J. Wu, R. Xu, Z. Yao, D. Wang, W. Tang, X. Wang, J. Tu, Porous Carbon Hosts for Lithium-Sulfur Batteries, Chem. Eur. J. 25 (2019) 3710, https://doi.org/10.1002/chem.201803153.
[53] H. Xu, Q. Jiang, B. Zhang, C. Chen, Z. Lin, Integrating Conductivity, Immobility, and Catalytic Ability into High-N Carbon/Graphene Sheets as an Effective Sulfur Host, Adv. Mater. 32 (2020), https://doi.org/10.1002/adma.201906357 e1906357.
[54] R.A. Abdul, X. Yuan, Y. Chen, J. Hu, Q. Mu, Y. Ma, X. Zhao, L. Miao, J.H. Ahn, Y. Peng, Z. Deng, Anchoring MOF-Derived CoS_2 on Sulfurized Polyacrylonitrile Nanofibers for High Areal Capacity Lithium-Sulfur Batteries, J. Mater. Chem. A 8 (2020) 1298, https://doi.org/10.1039/c9ta11390h.
[55] Y.T. Liu, D.D. Han, L. Wang, G.R. Li, S. Liu, X.P. Gao, $NiCo_2O_4$ Nanofibers as Carbon-Free Sulfur Immobilizer to Fabricate Sulfur-Based Composite with High Volumetric Capacity for Lithium-Sulfur Battery, Adv. Energy Mater. 9 (2019), https://doi.org/10.1002/aenm.201803477 1803477.
[56] Y.J. Oh, J.H. Kim, Y.C. Kang, Yolk–Shell-Structured Manganese Oxide/Nitride Composite Powders Comprising Cobalt-Nanoparticle-Embedded Nitrogen-Doped Carbon Nanotubes as Cathode Catalysts for Long-Life-Cycle Lithium-Oxygen Batteries, Chem. Eng. J. 373 (2019) 86, https://doi.org/10.1016/j.cej.2019.05.020.
[57] Y. Lin, Z. Qiu, D. Li, S. Ullah, Y. Hai, H. Xin, W. Liao, B. Yang, H. Fan, J. Xu, C. Zhu, NiS_2@CoS_2 Nanocrystals Encapsulated in N-Doped Carbon Nanocubes for High Performance Lithium/Sodium Ion Batteries, Energy Storage Mater. 11 (2018) 67, https://doi.org/10.1016/j.ensm.2017.06.001.
[58] S. Huang, Y.V. Lim, X. Zhang, Y. Wang, Y. Zheng, D. Kong, M. Ding, S.A. Yang, H. Y. Yang, Regulating the Polysulfide Redox Conversion by Iron Phosphide Nanocrystals for High-Rate and Ultrastable Lithium-Sulfur Battery, Nano Energy 51 (2018) 340, https://doi.org/10.1016/j.nanoen.2018.06.052.
[59] J. Xu, W. Zhang, H. Fan, F. Cheng, D. Su, G. Wang, Promoting Lithium Polysulfide/Sulfide Redox Kinetics by the Catalyzing of Zinc Sulfide for High Performance Lithium-Sulfur Battery, Nano Energy 51 (2018) 73, https://doi.org/10.1016/j.nanoen.2018.06.046.
[60] J. Cai, J. Jin, Z. Fan, C. Li, Z. Shi, J. Sun, Z. Liu, 3D Printing of a V_8C_7-VO_2 Bifunctional Scaffold as an Effective Polysulfide Immobilizer and Lithium Stabilizer for Li-S Batteries, Adv. Mater. (2020), https://doi.org/10.1002/adma.202005967 e2005967.
[61] W. Qiu, G. Li, D. Luo, Y. Zhang, Y. Zhao, G. Zhou, L. Shui, X. Wang, Z. Chen, Hierarchical Micro-Nanoclusters of Bimetallic Layered Hydroxide Polyhedrons as Advanced Sulfur Reservoir for High-Performance Lithium-Sulfur Batteries, Adv. Sci. (Weinh) 8 (2021), https://doi.org/10.1002/advs.202003400 2003400.
[62] S.D. Seo, S. Yu, S. Park, D.W. Kim, In Situ Conversion of Metal-Organic Frameworks into VO_2-V_3S_4 Heterocatalyst Embedded Layered Porous Carbon as an "All-in-One" Host for Lithium-Sulfur Batteries, Small 16 (2020), https://doi.org/10.1002/smll.202004806 e2004806.
[63] X. Yang, S. Chen, W. Gong, X. Meng, J. Ma, J. Zhang, L. Zheng, H.D. Abruna, J. Geng, Kinetic Enhancement of Sulfur Cathodes by N-Doped Porous Graphitic Carbon with Bound VN Nanocrystals, Small 16 (2020), https://doi.org/10.1002/smll.202004950 e2004950.